Fast Alternatives to Taylor and Sachs Models for Rigid Perfectly Viscoplastic Polycrystals

J. Kalisch, A. Bertram

We consider polycrystals consisting of rigid perfectly viscoplastic single crystals. Instead of tracking the evolution of (a) many individual crystallite orientations we determine the evolution of (b) the Fourier coefficients of the orientation distribution. Apart from the truncation order, the transition from single to polycrystal constitutive equations is unique, it does not involve additional parameters. While the reference model (a) requires the solution of numerous small systems of non-linear ODEs, our model (b) provides a system of linear ODEs the size of which depends on the truncation order. Upon establishing a data base for the matrix of system (b), the computing time is decreased significantly as compared to (a).

This paper is meant to introduce the fundamentals of our model in terms of the underlying physical concepts and a compact and convenient notation. In addition, we introduce a class of alternative approaches that allow for a non-negative approximation of the orientation distribution and generalise the equations for the texture evolution to arbitrary sets of base functions.

1 Introduction

Objective. The focus of our work is on the evolution of the crystallographic texture and its influence on the anisotropy of the plastic behaviour of polycrystals. Since the crystallographic texture is in essence described by the *orientation distribution*, we shall use a single crystal model with the internal state being completely described by the *orientation*. Thus we considerrigid perfectly viscoplastic single crystals and polycrystals consisting of these. While the upper and lower bounds of crystal plasticity, i. e. the approaches devised by Taylor (1938) and Sachs (1928), have been studied extensively in academics, in terms of computational costs they are still too demanding to be applied in industrial forming simulations. Subsequently, we present a less demanding alternative.

Concerning the evolution of the crystallographic texture, we start from the approach by Böhlke (2006), but continue in different directions. As far as the stress strain-rate relation is concerned, we extend the results of Böhlke and Bertram (2003) and Böhlke (2004) to the general anisotropic case. For the *potentials* of strain-rate and stress this has been done by Tsotsova and Böhlke (2009b) and Tsotsova and Böhlke (2009a). We shall include their theoretical results along the lines.

From a superordinate point of view, our approach follows the strategy to condense the important information of the microstructure and microscale constitutive functions prior to the application. This is a computationally demanding procedure, but it needs to be done only once. The permanent costs of the resulting model are comparatively small. Other approaches following this strategy are, e.g., the CP DFT (crystal plasticity discrete Fourier transformation) suggested by Knezevic et al. (2009), the CP FFT (crystal plasticity fast Fourier transformation) investigated by Liu et al. (2010) and the NTFA (non-uniform transformation field analysis) dealt with by Fritzen and Böhlke (2011a) and Fritzen and Böhlke (2011b).

Outline. The paper is organised as follows: *Section 2* deals with the key mathematical tools of the subsequent analysis. It contains the representation of functions on $\mathcal{SO}_3$ which involves the invariant integration and the Fourier expansion. *Section 3* recasts the underlying general framework for rigid perfectly viscoplastic single crystals in terms of non-dimensional and dual variables. *Section 4* introduces the orientation distribution function and (locally) homogeneous processes. Then we discuss different models for rigid perfectly viscoplastic polycrystals. Böhlke's and our approach differ by the way the closure problem for the infinite number of texture coefficients is dealt with. We then introduce a class of alternative descriptions of the orientation distribution function in terms of harmonic tensors. This class allows for truncations that yield non-negative approximations of the orientation distribution function. Moreover, we establish the decomposition of the truncation error. *Section 5* lists various features of our approach that allow for a reduction of the computing time. This section is meant to be the outline

of a forthcoming paper which includes a detailed description of the reduction procedure. *Section 6* contains the example of a uniaxial tensile test. For tensile strains as large as 100 % we find our approach to agree well with the reference model (i.e. the truncation error is negligible) while the computing time is reduced by several orders of magnitude. *Section 7* generalises the homogenisation procedure in Section 4 to arbitrary sets of base functions on $\mathcal{SO}_3$.

Notation. Scalars, vectors, second-order tensors, and tensors of higher or arbitrary order are denoted like a, $\mathbf{a}$, $\mathbf{A}$, and $\mathbb{A}$, respectively, while $\underline{\mathbb{A}}$ and $\underline{\underline{\mathbb{A}}}$ denote a supervector and a supertensor, respectively - we shall give a more precise description of this concept later. The scalar, dyadic, Rayleigh and infinitesimal Rayleigh product are denoted by $\cdot$, $\otimes$, $*$ and $\boxtimes$, respectively. For a given base $\{\mathbf{g}_i\}$ and an n-th order tensor $\mathbb{B} = B^{i_1 \cdots i_n} \mathbf{g}_{i_1} \otimes \ldots \otimes \mathbf{g}_{i_n}$ (mind Einstein's summation convention), the Rayleigh and infinitesimal Rayleigh product are given by

$$\mathbb{A} \cdot \mathbb{B} \quad = \quad A^{i_1 \cdots i_N} B_{i_1 \ldots i_N} \tag{1}$$

$$\mathbf{A} * \mathbb{B} \quad = \quad B^{i_1 \cdots i_n} \mathbf{A}[\mathbf{g}_{i_1}] \otimes \ldots \mathbf{A}[\mathbf{g}_{i_n}] \tag{2}$$

$$\mathbf{A} \boxtimes \mathbb{B} \quad = \quad B^{i_1 \cdots i_n} \left(\mathbf{A}[\mathbf{g}_{i_1}] \otimes \mathbf{g}_{i_2} \otimes \ldots \otimes \mathbf{g}_{i_n} + \ldots + \mathbf{g}_{i_1} \otimes \ldots \otimes \mathbf{g}_{i_{n-1}} \otimes \mathbf{A}[\mathbf{g}_{i_n}] \right) \tag{3}$$

where $[\ ]$ indicates the linear mapping (complete contraction of all lower order tensor indices) defined via

$$\mathbb{A}\,[\,\mathbb{B}\,] = A^{i_1 \cdots i_M j_1 \cdots j_N} B_{j1 \ldots jN} \ \mathbf{g}_{i_1} \otimes \ldots \otimes \mathbf{g}_{i_M} \tag{4}$$

The Frobenius norm for tensors of arbitrary order is defined by $\| A \| := (A \cdot A)^{\frac{1}{2}}$. To our knowledge, the operation $\boxtimes$ does not have an official name, currently. It comes in handy whenever derivatives of the Rayleigh product are required which is, why we have called it infinitesimal Rayleigh product.

Orientations and rotations are denoted by $\mathbf{Q}$ and $\mathbf{R}$, respectively. The difference between them is a subtle one, similar to that between a point in space (or a position vector) and an ordinary vector. Rotations connect orientations as vectors connect points. Groups are denoted like $\mathcal{G}$. In particular, $\mathcal{SO}_3$ is the group of proper rotations in a three-dimensional space.

2 Functions on $\mathcal{SO}_3$

Invariant integration on $\mathcal{SO}_3$. For locally compact groups, such as $\mathcal{SO}_3$, there exists a Háar measure. For our problem, it suffices to know that this implies the existence of an invariant differential form $d\mu(\mathbf{Q})$ giving rise to a left, right and inversion invariant normalised integration

$$\forall \mathbf{R} \in \mathcal{SO}_3 : \quad \int_{\mathcal{SO}_3} \mathbb{G}(\mathbf{R}\,\mathbf{Q})\,d\mu(\mathbf{Q}) \quad = \quad \int_{\mathcal{SO}_3} \mathbb{G}(\mathbf{Q})\,d\mu(\mathbf{Q}) \quad \text{left invariance} \tag{5}$$

$$\forall \mathbf{R} \in \mathcal{SO}_3 : \quad \int_{\mathcal{SO}_3} \mathbb{G}(\mathbf{Q}\,\mathbf{R})\,d\mu(\mathbf{Q}) \quad = \quad \int_{\mathcal{SO}_3} \mathbb{G}(\mathbf{Q})\,d\mu(\mathbf{Q}) \quad \text{right inv.} \tag{6}$$

$$\int_{\mathcal{SO}_3} \mathbb{G}(\mathbf{Q}^{-1})\,d\mu(\mathbf{Q}) \quad = \quad \int_{\mathcal{SO}_3} \mathbb{G}(\mathbf{Q})\,d\mu(\mathbf{Q}) \quad \text{inversion inv.} \tag{7}$$

$$\int_{\mathcal{SO}_3} 1\,d\mu(\mathbf{Q}) \quad = \quad 1 \quad \text{normalisation} \tag{8}$$

where $\mathbb{G}$ is an arbitrary (possibly tensor-valued) function. On a modest level, we may understand Eqs. 5-7 by considering the integration along a circle: neither the sense of integration nor the starting point affect the result. In this context, the circle represents the set of a group, e.g., the unit circle $\{\exp(i\,\phi)|\phi \in [0, 2\pi[\}$ in the plane of complex numbers; the group operation then is the usual multiplication of complex numbers. For more information on the subject we refer to Elstrodt (2009) and Gel'fand et al. (1963).

Fourier expansion on $\mathcal{SO}_3$. If the function $\mathbb{G}$ is square-integrable, it allows for a Fourier expansion (Adams et al. (1992), Guidi et al. (1992), Sam et al. (1993)). The expansion involves Fourier coefficients $\{\mathbb{G}_{m_\alpha}\}$ and mutually orthogonal base functions $\{\mathbb{B}_{m_\alpha}\}$. The latter are related to mutually orthogonal base tensors $\{\mathbb{H}_{m_\alpha}\}$ by virtue of the orientation $\mathbf{Q}$. Both $\mathbb{B}_{m_\alpha}$ and $\mathbb{H}_{m_\alpha}$ are harmonic (i.e. completely symmetric and deviatoric) tensors

of order m.

$$\int_{\mathcal{SO}_3} \| \, \mathbb{G}(\mathbf{Q}) \, \|^2 \, \mathrm{d}\mu(\mathbf{Q}) \quad < \quad \infty \tag{9}$$

$$\Rightarrow \quad \mathbb{G}(\mathbf{Q}) \quad = \quad \sum_{m=0}^{\infty} \sum_{\alpha=1}^{2\,m+1} \mathbb{G}_{m_\alpha} \left[\, \mathbb{B}_{m_\alpha}(\mathbf{Q}) \, \right] \tag{10}$$

$$\mathbb{G}_{m_\alpha} \quad := \quad \int_{\mathcal{SO}_3} \mathbb{G}(\mathbf{Q}) \otimes \mathbb{B}_{m_\alpha}(\mathbf{Q}) \, \mathrm{d}\mu(\mathbf{Q}) \tag{11}$$

$$\mathbb{B}_{m_\alpha}(\mathbf{Q}) \quad := \quad \mathbf{Q} * \mathbb{H}_{m_\alpha} \tag{12}$$

Harmonic base tensors. The set of $2\,m+1$ base tensors span the space of all harmonic tensors of order m. Consequently, we can express $\mathbb{I}_m$ - the identity on the space of harmonic tensors of order m - in terms of the base tensors,

$$\mathbb{H}_{m_\alpha} \cdot \mathbb{H}_{m_\beta} \quad = \quad (2\,m+1)\,\delta_{\alpha\beta} \tag{13}$$

$$\sum_{\alpha=1}^{2\,m+1} \mathbb{H}_{m_\alpha} \otimes \mathbb{H}_{m_\alpha} \quad = \quad (2\,m+1)\,\mathbb{I}_m \tag{14}$$

Base functions on $\mathcal{SO}_3$. The Dirac distribution δ and the identity on harmonic tensors are related to the base functions via

$$\delta(\mathbf{Q}, \mathbf{Q}') \quad := \quad \sum_{m=0}^{\infty} \sum_{\alpha=1}^{2\,m+1} \mathbb{B}_{m_\alpha}(\mathbf{Q}) \cdot \mathbb{B}_{m_\alpha}(\mathbf{Q}') \tag{15}$$

$$\int_{\mathcal{SO}_3} \mathbb{B}_{m_\alpha}(\mathbf{Q}) \otimes \mathbb{B}_{n_\beta}(\mathbf{Q}) \, \mathrm{d}\mu(\mathbf{Q}) \quad = \quad \delta_{mn}\,\delta_{\alpha\beta}\,\mathbb{I}_m \tag{16}$$

The Fourier expansion (Eqs. 10-11) is then easily understood by considering

$$\mathbb{G}(\mathbf{Q}) = \int_{\mathcal{SO}_3} \mathbb{G}(\mathbf{Q}')\,\delta(\mathbf{Q}', \mathbf{Q})\,\mathrm{d}\mu(\mathbf{Q})' \tag{17}$$

Scalar product. The scalar product of two square-integrable functions, $\mathbb{F}$ and $\mathbb{G}$, is given by

$$\int_{\mathcal{SO}_3} \mathbb{F}(\mathbf{Q}) \cdot \mathbb{G}(\mathbf{Q}) \, \mathrm{d}\mu(\mathbf{Q}) = \sum_{m=0}^{\infty} \sum_{\alpha=1}^{2\,m+1} \mathbb{F}_{m_\alpha} \cdot \mathbb{G}_{m_\alpha} \tag{18}$$

Supervectors and supertensors. Subsequently, we shall use more compact expressions such as

$$\mathbb{G}(\mathbf{Q}) \quad \overset{(10)}{=} \quad \underline{\mathbb{G}} \left[\, \underline{\mathbb{B}}(\mathbf{Q}) \, \right] \tag{19}$$

$$\underline{\mathbb{G}} \quad \overset{(11)}{:=} \quad \int \mathbb{G}(\mathbf{Q}) \otimes \underline{\mathbb{B}}(\mathbf{Q}) \, \mathrm{d}\mu(\mathbf{Q}) \tag{20}$$

$$\underline{\mathbb{B}}(\mathbf{Q}) \quad \overset{(12)}{:=} \quad \mathbf{Q} * \underline{\mathbb{H}} \tag{21}$$

$$\delta(\mathbf{Q}, \mathbf{Q}') \quad \overset{(15)}{:=} \quad \underline{\mathbb{B}}(\mathbf{Q}) \cdot \underline{\mathbb{B}}(\mathbf{Q}') \tag{22}$$

$$\int \underline{\mathbb{B}}(\mathbf{Q}) \otimes \underline{\mathbb{B}}(\mathbf{Q}) \, \mathrm{d}\mu(\mathbf{Q}) \quad \overset{(16)}{=} \quad \underline{\underline{\mathbb{I}}} \tag{23}$$

$$\int \mathbb{F}(\mathbf{Q}) \cdot \mathbb{G}(\mathbf{Q}) \, \mathrm{d}\mu(\mathbf{Q}) \quad \overset{(18)}{=} \quad \underline{\mathbb{F}} \cdot \underline{\mathbb{G}} \tag{24}$$

Here, $\underline{\mathbb{B}}$, $\underline{\mathbb{F}}$, $\underline{\mathbb{G}}$ and $\underline{\mathbb{H}}$ are supervectors, while the identity $\underline{\underline{\mathbb{I}}}$ is a second-order supertensor satisfying, e.g., $\underline{\underline{\mathbb{I}}}\,[\,\underline{\mathbb{G}}\,] = \underline{\mathbb{G}}$. We have introduced this compact notation in order not to conceal the essential structure of the equations in the subsequent sections.

3 Rigid Perfectly Viscoplastic Single Crystals

Locally homogeneous process. Throughout this work, we consider constitutive functions at time t and material point $\mathbf{x}_0$ (i.e. a material volume comprising $\mathbf{x}_0$ and being sufficiently small in comparison to the length scales

across which the process variables $\mathbf{W}$ and $\mathbf{X}$ change significantly and yet large enough to include all important features of the crystallographic texture). However, we shall suppress the arguments $\mathbf{x}_0$ and t whenever possible. The term locally homogeneous process is used subsequently to emphasize that within such a volume, the process variables are assumed homogeneous, but they may still vary from one material point to another.

Single crystal model. The mechanical behaviour of rigid perfectly viscoplastic single crystals is specified by two constitutive functions, $\mathbf{A}$ and $\mathbf{S}$, mapping second-order harmonic tensors to second-order skew and second-order harmonic tensors, respectively. More precisely, we have

$$\dot{\mathbf{Q}}\,\mathbf{Q}^{\mathrm{T}} \;=\; \mathbf{W} - \dot{\gamma}_0\,\mathbf{Q}\,\mathbf{A}\,(\mathbf{Q}^{\mathrm{T}}\mathbf{X}\,\mathbf{Q})\,\mathbf{Q}^{\mathrm{T}} \tag{25}$$

$$\mathbf{X}_\dagger \;=\; \mathbf{Q}\,\mathbf{S}\,(\mathbf{Q}^{\mathrm{T}}\mathbf{X}\,\mathbf{Q})\,\mathbf{Q}^{\mathrm{T}} \tag{26}$$

where Eq. 25 describes the evolution of the lattice orientation $\mathbf{Q}$ for a given $\mathbf{W}$-$\mathbf{X}$-process, while Eq. 26 relates the dual variables, $\mathbf{X}$ and $\mathbf{X}_\dagger$ (see, e.g., Hutchinson (1976), Böhlke and Bertram (2003), Böhlke (2004)).
The dual variables correspond to the non-dimensional strain rate deviator $\frac{\mathbf{D}'}{\dot{\gamma}_0}$ and the Kirchhoff stress deviator $\frac{\mathbf{T}'}{\tau_{\mathrm{c}}}$ or vice versa. The material parameters $\dot{\gamma}_0$ and τ_{c} are called critical shear rate and critical resolved shear stress, respectively. In addition, we can introduce a non-dimensional spin $\frac{\mathbf{W}}{\dot{\gamma}_0}$ and a non-dimensional time increment $\mathrm{d}\gamma := \dot{\gamma}_0\,\mathrm{d}t$.

Duality. The term *dual* is further emphasized by the following considerations: If $\mathbf{A}$, $\mathbf{S}$ are given explicitly in terms of $\mathbf{X}$ and the $\mathbf{W}$-$\mathbf{X}_\dagger$-process is prescribed, we can recover the same formulation by means of the dual functions $\mathbf{A}_\dagger$ and $\mathbf{S}_\dagger$ - provided $\mathbf{S}$ is bijective. Introducing the abbreviations $\mathbf{Y} := \mathbf{Q}^{\mathrm{T}}\mathbf{X}\,\mathbf{Q}$ and $\mathbf{Y}_\dagger := \mathbf{Q}^{\mathrm{T}}\mathbf{X}_\dagger\,\mathbf{Q}$, Eq. 26 is compactly rewritten as

$$\mathbf{Y}_\dagger = \mathbf{S}(\mathbf{Y}) \tag{27}$$

allowing to establish the dual functions by

$$\mathbf{S}_\dagger(\mathbf{Y}_\dagger) \;=\; \mathbf{S}^{-1}(\mathbf{Y}_\dagger) \tag{28}$$

$$\mathbf{A}_\dagger(\mathbf{Y}_\dagger) \;=\; \mathbf{A}\circ\mathbf{S}^{-1}(\mathbf{Y}_\dagger) \tag{29}$$

If, in addition, $\mathbf{S}$ has a convex potential $\psi = \mathrm{p}(\mathbf{Y})$, thus

$$\mathbf{S}(\mathbf{Y}) = \frac{\mathrm{dp}(\mathbf{Y})}{\mathrm{d}\mathbf{Y}} \tag{30}$$

then the dual potential $\psi_\dagger = \mathrm{p}_\dagger(\mathbf{Y}_\dagger)$ is obtained via the Legendre-Fenchel transformation and satisfies

$$\mathbf{S}_\dagger(\mathbf{Y}_\dagger) \;=\; \frac{\mathrm{dp}_\dagger(\mathbf{Y}_\dagger)}{\mathrm{d}\mathbf{Y}_\dagger} \tag{31}$$

$$\mathrm{p}_\dagger(\mathbf{Y}_\dagger) \;=\; \sup_{\mathbf{Z}}\,(\mathbf{Z}\cdot\mathbf{Y}_\dagger - \mathrm{p}(\mathbf{Z})) \tag{32}$$

$$\;=\; \mathbf{Y}\cdot\mathbf{Y}_\dagger - \mathrm{p}(\mathbf{Y}) \quad\text{where}\quad \mathbf{Y} = \mathbf{S}_\dagger(\mathbf{Y}_\dagger) \tag{33}$$

Moreover, we assume $\mathbf{A}$ and $\mathbf{S}$ (and thus p) continuously differentiable and bounded - and thus square-integrable on $\mathcal{SO}_3$ - for finite $\mathbf{X}$ and arbitrary orientations.

Dissipation. The non-dimensional dissipation η is given by the scalar product of the dual variables and has to be non-negative. If p is convex, the non-negativity is ensured.

$$\eta \;:=\; \frac{\mathbf{T}'}{\tau_{\mathrm{c}}}\cdot\frac{\mathbf{D}'}{\dot{\gamma}_0} \tag{34}$$

$$\;=\; \mathbf{X}\cdot\mathbf{X}_\dagger \tag{35}$$

$$\;=\; \mathbf{Y}\cdot\mathbf{Y}_\dagger \tag{36}$$

$$\;=\; \mathrm{p}(\mathbf{Y}) + \mathrm{p}_\dagger(\mathbf{Y}_\dagger) \tag{37}$$

$$\;=\; \psi + \psi_\dagger \tag{38}$$

In the transition from Eq. 36 to Eq. 37, Eq. 33 has been used.

4 Rigid Perfectly Viscoplastic Polycrystals

Orientation distribution function. The crystallographic texture can be described by means of the orientation distribution function (ODF) f, which, by definition, gives the volume fraction of single crystals (or grains) with a similar lattice orientation (Bunge (1965))

$$f(\mathbf{Q})\, d\mu(\mathbf{Q}) = \frac{dV(\mathbf{Q}, d\mu(\mathbf{Q}))}{V} \tag{39}$$

The ODF is normalised and non-negative

$$\int f(\mathbf{Q})\, d\mu(\mathbf{Q}) = 1 \tag{40}$$

$$\forall\, \mathbf{Q} \in \mathcal{SO}_3: \quad f(\mathbf{Q}) \geq 0 \tag{41}$$

Furthermore, texture and crystal symmetries (with groups $\mathcal{G}_T, \mathcal{G}_C \subset \mathcal{SO}_3$) imply

$$\forall\, \mathbf{R}_T \in \mathcal{G}_T: \quad f(\mathbf{R}_T\, \mathbf{Q}) = f(\mathbf{Q}) \tag{42}$$

$$\forall\, \mathbf{R}_C \in \mathcal{G}_C: \quad f(\mathbf{Q}\, \mathbf{R}_C) = f(\mathbf{Q}) \tag{43}$$

The Fourier coefficients of the ODF are called texture coefficients $\mathbb{T}$.

$$f(\mathbf{Q}) = \mathbb{T} \cdot \mathbb{B}(\mathbf{Q}) \tag{44}$$

$$\mathbb{T} := \int f(\mathbf{Q})\, \mathbb{B}(\mathbf{Q})\, d\mu(\mathbf{Q}) \tag{45}$$

If the ODF is time dependent, then $f(\mathbf{Q}, t) = \mathbb{T}(t) \cdot \mathbb{B}(\mathbf{Q})$ etc. as in the following sections.

The existence of a motion and its implications. For the sake of brevity we define the lattice spin function $\mathbf{\Omega}$

$$\mathbf{\Omega}\,(\mathbf{Q}, \mathbf{W}, \mathbf{X}) := \mathbf{W} - \dot{\gamma}_0\, \mathbf{Q}\, \mathbf{A}\, (\mathbf{Q}^T \mathbf{X}\, \mathbf{Q})\, \mathbf{Q}^T \tag{46}$$

If $\mathbf{A}$ is continuously differentiable and the $\mathbf{W}$-$\mathbf{X}$-process is piecewise continuous, then the Picard-Lindelöf theorem implies the existence and uniqueness of a continuous solution $\mathbf{Q}(t)$. The uniqueness implies that trajectories starting from different initial values cannot intersect at finite time. However, they may converge towards a common limit. Thus, considering the set of all trajectories for a given $\mathbf{W}$-$\mathbf{X}$-process, we find - at any time - a unique relation between initial and current orientations.

This corresponds exactly to the concept of a motion χ of material points in continuum mechanics (see, e.g., Bertram (2012)), however, now in $\mathcal{SO}_3$ with the initial orientations $\mathbf{Q}_0$ corresponding to material coordinates.

$$\mathbf{Q}(t) = \chi(\mathbf{Q}_0, t) \tag{47}$$

Since all initial orientations are assumed to be subject to the same $\mathbf{W}$-$\mathbf{X}$-process, our analysis is restricted to locally homogeneous processes - in other words, to Taylor and Sachs models.

Texture evolution. Using the concept of a motion, Böhlke (Böhlke (2006)) has shown that the evolution of the texture coefficients is given by

$$\dot{\mathbb{T}} = \int \mathbf{\Omega} \boxtimes \mathbb{B}\, f\, d\mu(\mathbf{Q}) \tag{48}$$

which by means of Eq. 44 is rewritten as a linear ODE for the texture coefficients

$$\dot{\mathbb{T}} = \mathbb{L}\,[\,\mathbb{T}\,] \tag{49}$$

$$\mathbb{L} := \int (\mathbf{\Omega} \boxtimes \mathbb{B}) \otimes \mathbb{B}\, d\mu(\mathbf{Q}) \tag{50}$$

The decomposition of the lattice spin (Eq. 46) into $\mathbf{W}$- and $\mathbf{X}$-dependent part also translates to the evolution of $\mathbb{T}$. As for single crystals, the $\mathbf{W}$-dependent parts accounts for rigid body motions.

$$\underline{\mathbb{L}}(\mathbf{W}, \mathbf{X})\,[\mathbb{T}] \quad = \quad \mathbf{W} \boxtimes \mathbb{T} - \dot{\gamma}_0\,\underline{\mathbb{A}}(\mathbf{X})\,[\mathbb{T}] \tag{51}$$

$$\underline{\mathbb{A}}(\mathbf{X}) \quad := \quad \int \left(\check{\mathbf{A}}(\mathbf{Q}, \mathbf{X}) \boxtimes \underline{\mathbb{B}}(\mathbf{Q})\right) \otimes \underline{\mathbb{B}}(\mathbf{Q})\,\mathrm{d}\mu(\mathbf{Q}) \tag{52}$$

$$\check{\mathbf{A}}(\mathbf{Q}, \mathbf{X}) \quad := \quad \mathbf{Q}\,\mathbf{A}\,(\mathbf{Q}^{\mathrm{T}}\mathbf{X}\,\mathbf{Q})\,\mathbf{Q}^{\mathrm{T}} \tag{53}$$

Stress strain-rate relation. For locally homogeneous processes we can transform volume averages to orientation averages via Eq. 39. Consequently, the volume average of the potential (Tsotsova and Böhlke (2009b), Tsotsova and Böhlke (2009a)) and the volume average of the dual variable are given by

$$\Psi \quad = \quad \int \mathrm{p}(\mathbf{Q}^{\mathrm{T}}\mathbf{X}\,\mathbf{Q})\,\mathrm{f}(\mathbf{Q}, \mathrm{t})\,\mathrm{d}\mu(\mathbf{Q}) \tag{54}$$

$$\mathbf{X}_\dagger \quad = \quad \int \check{\mathbf{S}}(\mathbf{Q}, \mathbf{X})\,\mathrm{f}(\mathbf{Q}, \mathrm{t})\,\mathrm{d}\mu(\mathbf{Q}) \tag{55}$$

$$\check{\mathbf{S}}(\mathbf{Q}, \mathbf{X}) \quad := \quad \mathbf{Q}\,\mathbf{S}\,(\mathbf{Q}^{\mathrm{T}}\mathbf{X}\,\mathbf{Q})\,\mathbf{Q}^{\mathrm{T}} \tag{56}$$

According to Eq. 24, the right hand sides are scalar products and can be rewritten as follows

$$\Psi \quad = \quad \underline{\mathbb{P}}(\mathbf{X}) \cdot \mathbb{T} \tag{57}$$

$$\mathbf{X}_\dagger \quad = \quad \underline{\mathbb{S}}(\mathbf{X})\,[\mathbb{T}] \tag{58}$$

where the polycrystal constitutive functions $\underline{\mathbb{S}}$ and $\underline{\mathbb{P}}$ are given by

$$\underline{\mathbb{P}}(\mathbf{X}) \quad := \quad \int \mathrm{p}\,(\mathbf{Q}^{\mathrm{T}}\mathbf{X}\,\mathbf{Q})\,\underline{\mathbb{B}}(\mathbf{Q})\,\mathrm{d}\mu(\mathbf{Q}) \tag{59}$$

$$\underline{\mathbb{S}}(\mathbf{X}) \quad := \quad \int \check{\mathbf{S}}(\mathbf{Q}, \mathbf{X}) \otimes \underline{\mathbb{B}}(\mathbf{Q})\,\mathrm{d}\mu(\mathbf{Q}) \tag{60}$$

Since ψ and $\mathbf{X}_\dagger$ are related via derivatives (Eq. 30) in single crystals, so are Ψ and $\mathbf{X}_\dagger$ in polycrystals

$$\mathbf{X}_\dagger \quad = \quad \left.\frac{\partial\psi}{\partial\mathbf{X}}\right|_{\mathbf{Q}} \tag{61}$$

$$\mathbf{X}_\dagger \quad = \quad \left.\frac{\partial\Psi}{\partial\mathbf{X}}\right|_{\mathbb{T}} \tag{62}$$

4.1 Our Approach

The sum in, e.g., Eq. 10 involves an infinite number of terms, which is impractical to deal with. Therefore, we consider a finite subsystem of Eq. 49 and neglect the contribution of higher order texture coefficients with order $\mathrm{m} > \mathrm{M}$, where M is the truncation order. Our polycrystal model is thus given by

$$\dot{\mathbb{T}}_{\mathrm{M}} \quad = \quad \mathbf{W} \boxtimes \mathbb{T}_{\mathrm{M}} - \dot{\gamma}_0\,\underline{\underline{\mathbb{A}}}_{\mathrm{MM}}\,[\mathbb{T}_{\mathrm{M}}] \tag{63}$$

$$\Psi \quad = \quad \underline{\mathbb{P}}_{\mathrm{M}}(\mathbf{X}) \cdot \mathbb{T}_{\mathrm{M}} \tag{64}$$

$$\mathbf{X}_\dagger \quad = \quad \underline{\mathbb{S}}_{\mathrm{M}}(\mathbf{X})\,[\mathbb{T}_{\mathrm{M}}] \tag{65}$$

where

$$\underline{\underline{\mathbb{A}}}_{\mathrm{MM}}(\mathbf{X}) \quad := \quad \int (\check{\mathbf{A}}(\mathbf{Q}, \mathbf{X}) \boxtimes \underline{\mathbb{B}}_{\mathrm{M}}(\mathbf{Q})) \otimes \underline{\mathbb{B}}_{\mathrm{M}}(\mathbf{Q})\,\mathrm{d}\mu(\mathbf{Q}) \tag{66}$$

$$\underline{\mathbb{P}}_{\mathrm{M}}(\mathbf{X}) \quad := \quad \int \mathrm{p}\,(\mathbf{Q}^{\mathrm{T}}\mathbf{X}\,\mathbf{Q})\,\underline{\mathbb{B}}_{\mathrm{M}}(\mathbf{Q})\,\mathrm{d}\mu(\mathbf{Q}) \tag{67}$$

$$\underline{\mathbb{S}}_{\mathrm{M}}(\mathbf{X}) \quad := \quad \int \check{\mathbf{S}}(\mathbf{Q}, \mathbf{X}) \otimes \underline{\mathbb{B}}_{\mathrm{M}}(\mathbf{Q})\,\mathrm{d}\mu(\mathbf{Q}) \tag{68}$$

In terms of the ODF, this truncation corresponds to projecting the ODF on a subspace

$$f \to f_M := \underline{\mathbb{T}}_M \cdot \underline{\mathbb{B}}_M \tag{69}$$

Depending on the single crystal functions $\mathbf{A}$ and $\mathbf{S}$, we choose a truncation order that renders a reasonable agreement for a set of test processes.

4.2 Reference Model

The reference model (Sachs or Taylor, upper index R) consists of a sufficiently large number K of single crystals with volume fractions f_k and orientations $\mathbf{Q}_k$. The orientations evolve according to Eqs. 25 and 26 and are subject to the same $\mathbf{W}$-$\mathbf{X}$-process,

$$\dot{\mathbf{Q}}_k \, \mathbf{Q}_k^{\mathrm{T}} = \mathbf{W} - \dot{\gamma}_0 \, \check{\mathbf{A}}(\mathbf{Q}_k, \mathbf{X}) \tag{70}$$

$$\Psi^{\mathrm{R}} = \sum_{k=1}^{K} f_k \, \mathrm{p}(\mathbf{Q}_k^{\mathrm{T}} \mathbf{X} \, \mathbf{Q}_k) \tag{71}$$

$$\mathbf{X}_\dagger^{\mathrm{R}} = \sum_{k=1}^{K} f_k \, \check{\mathbf{S}}(\mathbf{Q}_k, \mathbf{X}) \tag{72}$$

The respective ODF and texture coefficients are given by

$$f^{\mathrm{R}}(\mathbf{Q}) = \sum_{k=1}^{K} f_k \, \delta(\mathbf{Q}, \mathbf{Q}_k) \tag{73}$$

$$\underline{\mathbb{T}}_{(M)}^{\mathrm{R}} = \sum_{k=1}^{K} f_k \, \underline{\mathbb{B}}_{(M)}(\mathbf{Q}_k) \tag{74}$$

4.3 Decomposition of the Truncation Error

Comparing the results of the reference model (Sect. 4.2) to those of our approach, we find the following decomposition of the truncation error

$$\Psi - \Psi^{\mathrm{R}} = \underline{\mathbb{P}}_M(\mathbf{X}) \cdot \left(\underline{\mathbb{T}}_M - \underline{\mathbb{T}}_M^{\mathrm{R}}\right) + \left(\underline{\mathbb{P}}_M(\mathbf{X}) - \underline{\mathbb{P}}(\mathbf{X})\right) \cdot \underline{\mathbb{T}}^{\mathrm{R}} \tag{75}$$

$$\leq \|\underline{\mathbb{P}}_M(\mathbf{X})\| \underbrace{\|\underline{\mathbb{T}}_M - \underline{\mathbb{T}}_M^{\mathrm{R}}\|}_{=:\varepsilon_M^{\mathrm{T}}} + \underbrace{\|\underline{\mathbb{P}}_M(\mathbf{X}) - \underline{\mathbb{P}}(\mathbf{X})\|}_{=:\varepsilon_M^{\mathrm{P}}} \|\underline{\mathbb{T}}^{\mathrm{R}}\| \tag{76}$$

A similar decomposition applies to $\mathbf{X}_\dagger - \mathbf{X}_\dagger^{\mathrm{R}}$.

The term $\varepsilon_M^{\mathrm{P}}$ describes the error due to truncating the Fourier expansion of p. If p is polynomial in $\mathbf{Q}$, then its Fourier expansion is finite and $\varepsilon_M^{\mathrm{P}}$ is zero whenever the truncation order is chosen at least equal to the polynomial order. Otherwise, the error can be estimated using the equivalent expression

$$\varepsilon_M^{\mathrm{P}} = \left(\int_{\mathcal{SO}_3} \mathrm{p}^2(\mathbf{Q}^{\mathrm{T}} \mathbf{X} \, \mathbf{Q}) \, \mathrm{d}\mu(\mathbf{Q}) - \|\underline{\mathbb{P}}_M(\mathbf{X})\|^2\right)^{\frac{1}{2}} \tag{77}$$

Since the norm of $\underline{\mathbb{P}}_M$ increases as M does, the truncation error $\varepsilon_M^{\mathrm{P}}$ decreases monotonously, and, as p is square-integrable, it converges to zero

$$\varepsilon_M^{\mathrm{P}} \geq \varepsilon_{M+1}^{\mathrm{P}} \qquad \lim_{M \to \infty} \varepsilon_M^{\mathrm{P}} = 0 \tag{78}$$

By contrast, the term $\varepsilon_M^{\mathrm{T}}$ is the error in $\underline{\mathbb{T}}_M$ due to truncating the system of evolution equations The relation of truncation error and truncation order will be investigated in more detail in a forthcoming paper. For the time being we have to content ourselves with numerical examples to investigate this error.

4.4 Evolution of Non-negative ODF Approximations

Non-negative approximations. Working with an infinite number of texture coefficients is impractical. To circumvent this problem we may truncate the Fourier expansion, as has been done in the previous section. However, this can induce regions where the ODF becomes negative, thus violating the constraint of non-negativity (Eq. 41). An alternative approach ensuring non-negativity is described subsequently. First, we consider a continuously differentiable bijective non-negative function g

$$g : \mathbb{R} \to \mathbb{R}_0^+ \tag{79}$$

and, for the time being, an infinite vector of alternative texture coefficients $\underline{\mathbb{K}}$, similar to $\underline{\mathbb{T}}$. Then, the ODF is replaced by

$$f = g(\underline{\mathbb{K}} \cdot \underline{\mathbb{B}}) \tag{80}$$

Evolution of alternative texture coefficients. Based again on the concept of a motion, the respective evolution equations are given by

$$\underline{\underline{\mathbb{M}}}(\underline{\mathbb{K}}) \, [\, \dot{\underline{\mathbb{K}}}\,] \quad = \quad \underline{\underline{\mathbb{L}}}(\mathbf{W}, \mathbf{X}, \underline{\mathbb{K}}) \, [\, \underline{\mathbb{K}}\,] \tag{81}$$

$$\underline{\underline{\mathbb{M}}}(\underline{\mathbb{K}}) \quad := \quad \int G(\underline{\mathbb{K}} \cdot \underline{\mathbb{B}}) \, \underline{\mathbb{B}} \otimes \underline{\mathbb{B}} \, d\mu \tag{82}$$

$$\underline{\underline{\mathbb{L}}}(\mathbf{W}, \mathbf{X}, \underline{\mathbb{K}}) \quad := \quad \int (\mathbf{\Omega} \boxtimes \underline{\mathbb{B}}) \otimes \underline{\mathbb{B}} + (1 - G(\underline{\mathbb{K}} \cdot \underline{\mathbb{B}})) \, \underline{\mathbb{B}} \otimes (\mathbf{\Omega} \boxtimes \underline{\mathbb{B}}) \, d\mu \tag{83}$$

$$G(x) \quad := \quad \frac{x}{g(x)} \frac{dg(x)}{dx} \tag{84}$$

with second-order supertensors $\underline{\underline{\mathbb{M}}}$ and $\underline{\underline{\mathbb{L}}}$. In this context, $G = 1$ corresponds to our original approach.

Lattice spin decomposition. Using Eq. 46, we find the reduced system where the influence of $\mathbf{W}$ and $\mathbf{X}$ are separated

$$\underline{\underline{\mathbb{M}}}(\underline{\mathbb{K}}) \, [\, \dot{\underline{\mathbb{K}}} - \mathbf{W} \boxtimes \underline{\mathbb{K}}\,] = \underline{\underline{\mathbb{L}}}(0, \mathbf{X}, \underline{\mathbb{K}}) \, [\, \underline{\mathbb{K}}\,] \tag{85}$$

Invertible $\underline{\underline{\mathbb{M}}}$. If G is continuous and either non-negative or non-positive, then the linear mapping $\underline{\underline{\mathbb{M}}}$ is positive definite or negative definite, respectively. This implies invertibility and provides a system of non-linear first order ODEs

$$\dot{\underline{\mathbb{K}}} = \underline{\underline{\mathbb{M}}}^{-1}(\underline{\mathbb{K}}) \, \underline{\underline{\mathbb{L}}}(\mathbf{W}, \mathbf{X}, \underline{\mathbb{K}}) \, [\, \underline{\mathbb{K}}\,] \tag{86}$$

Polynomial approach. $\underline{\underline{\mathbb{M}}}$ is $\underline{\mathbb{K}}$-independent only if $G = c$ with constant c. This implies $g(x) := x^c$.

Homogeneity. Changing $g \to c\,g$ by a non-zero constant $c \neq 0$ does not alter G. Changing $g \to g^k$ renders $G \to k\,G$.

Exponential approach. The maximum entropy approximation (see Sect. 4.6) suggests to investigate $g(x) = \exp x$, which provides $G(x) = x$. In this case, $\underline{\underline{\mathbb{M}}}$ can become non-invertible and the evolution is given by a system of quasi-linear ODEs. We emphasize that this system does *not* describe the evolution of the pseudo-texture coefficients in Böhlke's approach (Sect. 4.6).

Truncation. Since g is non-negative by definition, we can perform the truncation $\underline{\mathbb{K}} \to \underline{\mathbb{K}}_M, \underline{\underline{\mathbb{M}}} \to \underline{\underline{\mathbb{M}}}_M, \underline{\underline{\mathbb{L}}} \to \underline{\underline{\mathbb{L}}}_M$ without violating non-negativity.

$$f \to f_M := g(\underline{\mathbb{K}}_M \cdot \underline{\mathbb{B}}_M) \geq 0 \tag{87}$$

Certainly, there will be a truncation error due to employing a truncated system of evolution equations. However, for an appropriate choice of G (and then g), an easier investigation of the related truncation error might be possible. The following remarks apply to arbitrary g (or G).

4.5 Quadratic Approximation

Among the recently introduced class of approximations, one strikes with particular simplicity: Choosing $g(x) = x^2$ (or $G = 2$), we obtain the evolution equation

$$\dot{\underline{\mathbb{K}}} \quad = \quad \underline{\underline{\mathbb{F}}} \, [\, \underline{\mathbb{K}}\,] \tag{88}$$

$$\underline{\underline{\mathbb{F}}} \quad := \quad \frac{1}{2} \int (\mathbf{\Omega} \boxtimes \underline{\mathbb{B}}) \otimes \underline{\mathbb{B}} - \underline{\mathbb{B}} \otimes (\mathbf{\Omega} \boxtimes \underline{\mathbb{B}}) \, d\mu \tag{89}$$

where the matrix $\underline{\underline{\mathbb{F}}}$ is exactly the skew part of the matrix in our approach (Sect. 4.1). This quadratic approximation has been suggested by van Houtte (1983) in a different setting to solve an altogether different question. The normalisation of the ODF implies $\|\underline{\mathbb{K}}\| = 1$ for any time, thus $\underline{\mathbb{K}}(t)$ differs from $\underline{\mathbb{K}}(0)$ merely by a rotation (in accordance with $\underline{\underline{\mathbb{F}}}$ being skew). This also applies to every subsystem emerging from the truncation procedure. The potential is rewritten as a positive definite quadratic form in $\underline{\mathbb{K}}$

$$\Psi \quad = \quad \underline{\underline{\mathbb{P}}}(\mathbf{X}) \cdot (\underline{\mathbb{K}} \otimes \underline{\mathbb{K}}) \tag{90}$$

$$\underline{\underline{\mathbb{P}}}(\mathbf{X}) \quad := \quad \int \mathrm{p}(\mathbf{Q}^{\mathrm{T}} \mathbf{X} \, \mathbf{Q}) \, \underline{\mathbb{B}}(\mathbf{Q}) \otimes \underline{\mathbb{B}}(\mathbf{Q}) \, \mathrm{d}\mu \tag{91}$$

4.6 Böhlke's Approach

An alternative approach based on a finite number of harmonic tensors and ensuring non-negativity of the approximate ODF, has been investigated by Böhlke (2006). In order to circumvent the closure problem, he considers a finite subvector of texture coefficients $\underline{\mathbb{T}}_{\mathrm{M}}$ (as we have done in our approach) and uses the maximum entropy method (Jaynes (1957a), Jaynes (1957b), Böhlke (2005), Junk et al.) to approximate f in the integral on the right hand side of Eq. 48. This yields an exponential function ensuring the non-negativity of the pseudo-ODF k_{M}. Upon replacing

$$\mathrm{f} \to \mathrm{k}_{\mathrm{M}} := \exp\left(\underline{\mathbb{K}}_{\mathrm{M}} \cdot \underline{\mathbb{B}}_{\mathrm{M}}\right) \tag{92}$$

the pseudo-texture coefficients $\underline{\mathbb{K}}_{\mathrm{M}}$ are uniquely determined by the constraints

$$\int \mathrm{k}_{\mathrm{M}} \, \underline{\mathbb{B}}_{\mathrm{M}} \, \mathrm{d}\mu = \underline{\mathbb{T}}_{\mathrm{M}} \tag{93}$$

In the respective examples provided by Böhlke (2006), the approach allows for a good prediction of the texture evolution even if the truncation order is as low as 6 or 8, i.e. only a small subvector $\underline{\mathbb{T}}_{\mathrm{M}}$ is taken into account. However, solving Eq. 93 for the auxiliary quantities $\underline{\mathbb{K}}_{\mathrm{M}}$ in every time increment is computationally demanding - even for truncation orders as low as these. For the sake of completeness we note that there exists no closed system of evolution equations for $\underline{\mathbb{K}}_{\mathrm{M}}$, such as $\underline{\mathbb{F}}_{\mathrm{M}}(\dot{\underline{\mathbb{K}}}_{\mathrm{M}}, \underline{\mathbb{K}}_{\mathrm{M}}, \mathbf{W}, \mathbf{X}) = 0$.

5 Reduction of the Computing Time

Since this section is intended to be merely an outline of a forthcoming paper, we shall only sketch the facts that help in reducing the computational costs. These facts also apply to the quadratic approximation (Sect. 4.4). For quick reference we restate our model

$$\dot{\underline{\mathbb{T}}}_{\mathrm{M}} \quad = \quad \underline{\underline{\mathbb{L}}}_{\mathrm{MM}}\left[\underline{\mathbb{T}}_{\mathrm{M}}\right] \tag{94}$$

$$\underline{\underline{\mathbb{L}}}_{\mathrm{MM}}(\mathbf{W}, \mathbf{X}) \quad := \quad \mathbf{W} \boxtimes -\dot{\gamma}_0 \, \underline{\underline{\mathbb{A}}}_{\mathrm{MM}}(\mathbf{X}) \tag{95}$$

$$\mathbf{X}_\dagger \quad = \quad \underline{\mathbb{S}}_{\mathrm{M}}(\mathbf{X})\left[\underline{\mathbb{T}}_{\mathrm{M}}\right] \tag{96}$$

$$\Psi \quad = \quad \underline{\mathbb{P}}_{\mathrm{M}}(\mathbf{X}) \cdot \underline{\mathbb{T}}_{\mathrm{M}} \tag{97}$$

where

$$\underline{\underline{\mathbb{A}}}_{\mathrm{MM}}(\mathbf{X}) \quad := \quad \left(\check{\mathbf{A}}(\mathbf{Q}, \mathbf{X}) \boxtimes \underline{\mathbb{B}}_{\mathrm{M}}(\mathbf{Q})\right) \otimes \underline{\mathbb{B}}_{\mathrm{M}}(\mathbf{Q}) \, \mathrm{d}\mu(\mathbf{Q}) \tag{98}$$

$$\underline{\mathbb{S}}_{\mathrm{M}}(\mathbf{X}) \quad := \quad \int \check{\mathbf{S}}(\mathbf{Q}, \mathbf{X}) \otimes \underline{\mathbb{B}}_{\mathrm{M}}(\mathbf{Q}) \, \mathrm{d}\mu(\mathbf{Q}) \tag{99}$$

$$\underline{\mathbb{P}}_{\mathrm{M}}(\mathbf{X}) \quad := \quad \int \mathrm{p}(\mathbf{Q}^{\mathrm{T}} \mathbf{X} \, \mathbf{Q}) \, \underline{\mathbb{B}}_{\mathrm{M}}(\mathbf{Q}) \, \mathrm{d}\mu(\mathbf{Q}) \tag{100}$$

There are two types of computational costs associated with our approach: initial costs and permanent costs.

5.1 Permanent Costs

Due to the time discretisation in numerical simulations, the piecewise continuous $\mathbf{W}$-$\mathbf{X}$-process is eventually replaced by a piecewise constant process which is in fact nothing but a sequence of monotonous subprocesses (or

increments for brevity). The update of $\mathbf{X}_\dagger$, Ψ and $\mathbb{T}_M$ along an increment gives rise to permanent costs.

Update. Given an increment $(\Delta t, \mathbf{W}, \mathbf{X})$ and initial values $\mathbb{T}_M(t)$, the task is to determine $\mathbb{T}_M(t + \Delta t)$ by virtue of Eq. 94 and then calculate $\mathbf{X}_\dagger(t + \Delta t)$ and $\Psi(t + \Delta t)$ using Eq. 96 and 97, respectively.

Analytic solution. The evolution equations form a system of linear ODEs. Thus, for any increment, there is an analytical solution.

$$\mathbb{T}_M(t + \Delta t) = \exp\left(\Delta t \, \underline{\underline{\mathbb{L}}}_{MM}\right)[\mathbb{T}_M(t)] \tag{101}$$

Depending on the process, the increments can become arbitrarily large. By contrast, in the reference model the increments are restricted by the problem of finding a solution to systems of non-linear equations.

The analytical solution (Eq. 101) involves the matrix exponential being applied to a vector. Usually, this can be computed even more efficiently than the matrix exponential itself. For more information on computing the matrix exponential we refer to Moler and van Loan (2003).

5.2 Initial Costs

The initial costs emerge from determining the data base. For a given single crystal model (and truncation order), the data base needs to be determined only once.

Data base. Obviously, the update requires to determine $\underline{\underline{\mathbb{L}}}_{MM}(\mathbf{W}, \mathbf{X})$, $\underline{\mathbb{S}}_M(\mathbf{X})$ and $\underline{\mathbb{P}}_M(\mathbf{X})$. The contribution of $\mathbf{W}$ to $\underline{\underline{\mathbb{L}}}_{MM}$ is trivial, thus we can consider $\underline{\underline{\mathbb{A}}}_{MM}(\mathbf{X})$ instead. If we had to evaluate these functions anew in every increment via their definition in terms of integrals over $\mathcal{SO}_3$ (Eqs. 98-100), our approach would easily be outperformed by the reference model. However, decomposing the variable $\mathbf{X}$ and invoking several symmetries of the functions, we can reconstruct the function values for any $\mathbf{X}$ from a small data base of function evaluations. This data base gives rise to the initial costs but reduces the permanent costs considerably.

Coaxial process. Within the aforementioned reconstruction, applying the rotation $\mathbf{R}$ (obtained from the decomposition $\mathbf{X} = \mathbf{R}\,\mathbf{X}_0\,\mathbf{R}^\mathrm{T}$) is by far the most time consuming operation. However, since we are interested in $\mathbf{X}_\dagger$ and Ψ rather than in the auxiliary quantities $\mathbb{T}$, we can introduce a coaxial process and coaxial quantities and thus circumvent this step. Again, this significantly reduces the permanent costs.

Zero elements. The first line of $\underline{\underline{\mathbb{A}}}$ is zero due to the normalisation of the ODF. The crystal symmetry renders certain lower order elements of $\underline{\mathbb{P}}$, $\underline{\mathbb{S}}$ and $\underline{\underline{\mathbb{A}}}$ zero. Also, the number of non-zero texture coefficients - and thus the size of the ODE system - is reduced considerably which, in turn, also reduces the permanent costs.

Depending on $\mathbf{A}$ and $\mathbf{S}$, the integrands in Eqs. 98-100 are reasonably well approximated by polynomials in the components of $\mathbf{Q}$. Then $\underline{\mathbb{P}}$ and $\underline{\mathbb{S}}$ are finite vectors, i.e. all elements are zero beyond some order related to the polynomial order. Likewise, the matrix $\underline{\underline{\mathbb{A}}}$ becomes a band matrix with the bandwidth related to that order. Of course, these findings apply likewise to the subvectors $\underline{\mathbb{P}}_M$ and $\underline{\mathbb{S}}_M$ and the submatrix $\underline{\underline{\mathbb{A}}}_{MM}$.

Independent components. The elements of $\underline{\mathbb{P}}$, $\underline{\mathbb{S}}$ and $\underline{\underline{\mathbb{A}}}$ are linear mappings from harmonic to harmonic tensors (real numbers can be referred to as harmonic tensors of order zero). In addition, they are invariant under all rotations that leave $\mathbf{X}$ invariant. This implies orthotropy for all elements of the data base. Once more this reduces the number of independent components to be evaluated.

6 Example

Schmid's law. Denoting slip direction and slip plane normal of slip system α by $\mathbf{d}_\alpha$ and $\mathbf{n}_\alpha$ (in an undistorted reference placement), respectively, we obtain antisymmetric and symmetric Schmid tensors, $\mathbf{A}_\alpha$ and $\mathbf{S}_\alpha$, by virtue of the additive decomposition

$$\mathbf{d}_\alpha \otimes \mathbf{n}_\alpha = \mathbf{A}_\alpha + \mathbf{S}_\alpha \tag{102}$$

Since $\mathbf{d}_\alpha \cdot \mathbf{n}_\alpha = 0$, we have $\mathrm{tr}\,\mathbf{S}_\alpha = 0$. The non-dimensional resolved shear stress on slip system α is given by

$$x_\alpha := \frac{\mathbf{Q}^\mathrm{T}\mathbf{T}'\,\mathbf{Q}}{\tau_c} \cdot \mathbf{S}_\alpha \tag{103}$$

and Schmid's law can be written as

$$\max_\alpha |x_\alpha| \le 1 \tag{104}$$

Hutchinson's flow rule. As a regularisation, Hutchinson (1976) proposed a power law with a strain-rate sensitivity parameter $q > 0$.

$$\mathbf{A} \quad = \quad \sum_\alpha \operatorname{sign} x_\alpha \, | \, x_\alpha \, |^q \, \mathbf{A}_\alpha \tag{105}$$

$$\mathbf{S} \quad = \quad \sum_\alpha \operatorname{sign} x_\alpha \, | \, x_\alpha \, |^q \, \mathbf{S}_\alpha \tag{106}$$

$$p \quad = \quad \frac{1}{q+1} \sum_\alpha | \, x_\alpha \, |^{q+1} \tag{107}$$

The larger q, the better is the approximation (of the shape) of Schmid's yield surface by the isolines of the flow potential p

$$\lim_{q \to \infty} \left(\frac{1}{q+1} \sum_\alpha | \, x_\alpha \, |^{q+1} \right)^{\frac{1}{q+1}} = \lim_{q \to \infty} \left(\sum_\alpha | \, x_\alpha \, |^{q+1} \right)^{\frac{1}{q+1}} = \max_\alpha | \, x_\alpha \, | \tag{108}$$

Uniaxial tensile test. We consider a polycrystal consisting of body-centred cubic (bcc) single crystals subject to uniaxial tension (stress controlled process - Sachs model) and apply Hutchinson's flow rule.
The crystal symmetry (cubic/octahedral, upper index C) renders several elements of $\mathbb{P}$, $\mathbb{S}$, $\mathbb{A}$ and $\mathbb{T}$ zero (see Sect. 5.2), reducing the list of relevant independent base functions to (see, e.g., Adams et al. (1992), Guidi et al. (1992), Böhlke (2005))

$$\underline{\mathbb{B}}^{C} = (\mathbb{B}_{0_1}, \mathbb{B}_{4_1}, \mathbb{B}_{6_1}, \mathbb{B}_{8_1}, \mathbb{B}_{9_1}, \mathbb{B}_{10_1}, \mathbb{B}_{12_1}, \mathbb{B}_{12_2}, \dots) \tag{109}$$

which is why we do not consider truncation order 1, 2, 3, 5, 7 and 11. Starting from isotropy

$$\underline{\mathbb{T}}_M(0) = (1, 0, \dots, 0) \tag{110}$$

and applying uniaxial tension (thus a transversely isotropic $\mathbf{X}$) with zero spin,

$$\mathbf{X} \quad = \quad \frac{\mathbf{T}'}{\tau_c} = \sqrt{\frac{2}{3}} \left(\mathbf{e}_1 \otimes \mathbf{e}_1 - \frac{1}{2} \mathbf{e}_2 \otimes \mathbf{e}_2 - \frac{1}{2} \mathbf{e}_3 \otimes \mathbf{e}_3 \right) \tag{111}$$

$$\mathbf{W} \quad = \quad 0 \tag{112}$$

all texture coefficients become transversely isotropic tensors. Being harmonic tensors at the same time, this renders all odd order texture coefficients zero and all even order texture coefficients having only one independent component. Here, we choose the $(1 \dots 1)$-component. This discards (truncation) order 9 from further consideration.

Analytical solution to our approach. Making use of these reductions and introducing the non-dimensional time $\gamma := \dot{\gamma}_0 \, t$, we end up with a small system of linear ODEs,

$$\frac{dT_i}{d\gamma} = - \sum_j A_{ij} \, T_j \qquad T = (T_0, T_4, T_6, T_8, T_{10}) \tag{113}$$

Evaluating the analytical solution

$$T_i(\gamma) = \sum_j \left(\exp(-\gamma A) \right)_{ij} \, T_j(0) \qquad T(0) = (1, 0, \dots, 0) \tag{114}$$

is a matter of split seconds and negligible when compared to the reference model.

Numerical results. Within any of the figures, the predictions for the evolution of one texture coefficient of order m based on different truncation orders M are given. Clearly, if the truncation order is, say, 6, then there are predictions for order 4 and 6 but not the evolution of the texture coefficients of order 8 and 10. The left (a) and right (b) column contain the plots of $(1 \dots 1)$-components of the texture coefficients and their difference to the reference model, $\Delta \underline{\mathbb{T}} := \underline{\mathbb{T}} - \underline{\mathbb{T}}^{R}$, respectively. The non-dimensional time γ (horizontal axis) is related to the nominal strain ε via

$$\varepsilon = \exp\left(\frac{2\gamma}{\sqrt{6}} \right) - 1 \tag{115}$$

M	line	γ	ε
4	black dashed	0.25	22.6 %
6	black dotted	0.50	50.4 %
8	black dot-dashed	0.75	84.5 %
10	black solid	1.00	126.3 %
R	grey solid	0.849	100.0 %

Here m and M denote the order of the texture coefficient and the truncation order, respectively.
In Fig. 2a and 3a, the black lines are almost indiscernible, i.e. the results for truncation orders 6, 8, 10 and 8, 10 coincide, respectively.
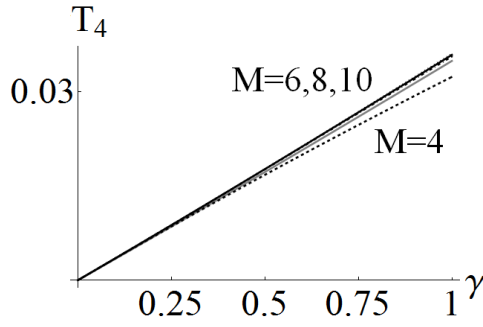
Fig.1a: $(1,\ldots,1)$-component of $\mathbb{T}_{4_1}$ vs. γ
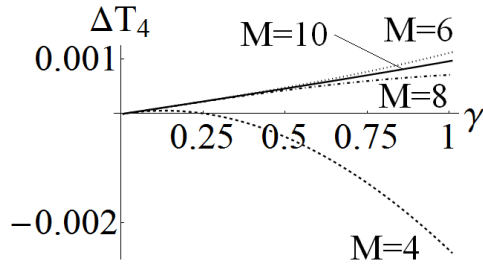
Fig.1b: $(1,\ldots,1)$-component of $\Delta\mathbb{T}_{4_1}$ vs. γ
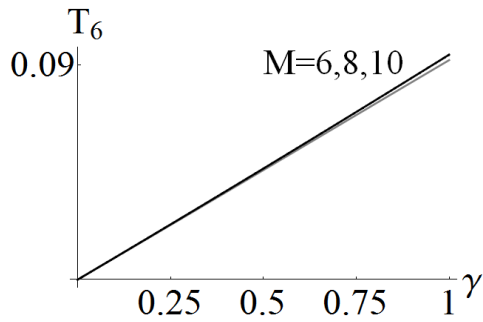
Fig.2a: $(1,\ldots,1)$-component of $\mathbb{T}_{6_1}$ vs. γ
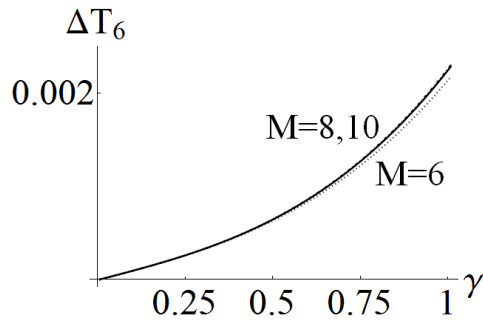
Fig.2b: $(1,\ldots,1)$-component of $\Delta\mathbb{T}_{6_1}$ vs. γ
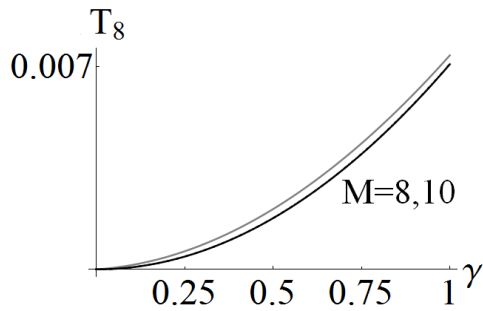
Fig.3a: $(1,\ldots,1)$-component of $\mathbb{T}_{8_1}$ vs. γ
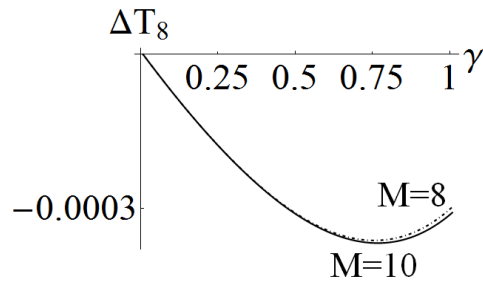
Fig.3b: $(1,\ldots,1)$-component of $\Delta\mathbb{T}_{8_1}$ vs. γ
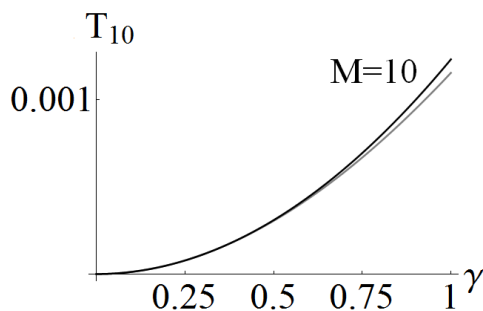
Fig.4a: $(1,\ldots,1)$-component of $\mathbb{T}_{10_1}$ vs. γ
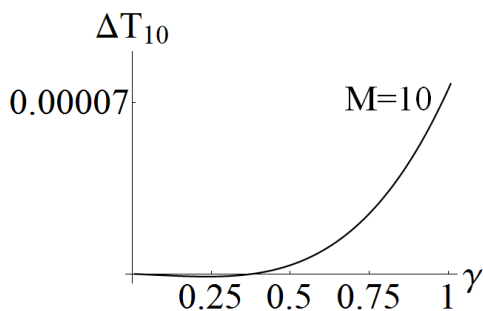
Fig.4b: $(1,\ldots,1)$-component of $\Delta\mathbb{T}_{10_1}$ vs. γ

Even for strains as large as 100%, the agreement between the reference model and our approach is quite convincing for truncation orders as low as six. However, having chosen $q = 3$, $\mathbf{X}_\dagger$ and Ψ contain coefficients up to order eight. Thus, only $M \geq 8$ provides $\varepsilon_M^P = 0$ (see Sect. 4.3).

Upon increasing the order, we expect the solutions to converge to those of the reference model. We find this assumption all in all confirmed by the example (see Fig.1a-4b) , but we shall discuss this issue in more detail in a forthcoming paper. Partly, deviations could be attributed to the initial values of higher order texture coefficients in the reference model, which are most likely non-zero.

Saturation. It may appear as if the all texture coefficients are bound to increase infinitely. However, since the first line of the matrix A and its submatrices is zero, they are singular and thus have at least one zero eigenvalue. The corresponding eigenvectors give stationary solutions.

7 Generalisation to Arbitrary Base Functions

Apart from the Fourier expansion in terms of harmonic tensors that was key to our model of rigid perfectly viscoplastic polycrystals, there are other sets of base functions, notably the generalised spherical harmonics (or Wigner D-functions) (see, e.g., Hielscher et al. (2010)). For some of these sets there already exist quite sophisticated codes. Therefore, we shall generalise our approach to a complete but otherwise arbitrary set of square-integrable base functions on $\mathcal{SO}_3$. Let $\mathcal{SO}_3$ be parametrised by three coordinates $\mathbf{q} = (q^1, q^2, q^3)$. The base functions $\{b^\alpha\}$ and dual base functions $\{b_\alpha\}$ fulfil

$$\sum_\alpha b^\alpha(\mathbf{q}) \, b_\alpha(\mathbf{q}') = \delta(\mathbf{q}, \mathbf{q}') \tag{116}$$

$$\int b^\alpha(\mathbf{q}) \, b_\beta(\mathbf{q}) \, d\mu(\mathbf{q}) = \delta_\beta^\alpha \tag{117}$$

The Fourier expansion and texture coefficients are given by

$$f(\mathbf{q}, t) = \sum_\alpha f^\alpha(t) \, b_\alpha(\mathbf{q}) \tag{118}$$

$$f^\alpha(t) := \int f(\mathbf{q}, t) \, b^\alpha(\mathbf{q}) \, d\mu(\mathbf{q}) \tag{119}$$

Thus, using eq. 35 in Böhlke (2006), the evolution of the coefficients is governed by (mind the implicit summation over i)

$$\frac{df^\alpha}{dt} = \frac{d}{dt} \int b^\alpha(\mathbf{q}) \, f(\mathbf{q}, t) \, d\mu(\mathbf{q}) \tag{120}$$

$$= \int \left. \frac{\partial b^\alpha(\mathbf{q})}{\partial t} \right|_{\mathbf{q}_0} f(\mathbf{q}, t) \, d\mu(\mathbf{q}) \tag{121}$$

$$= \int \left(\frac{\partial b^\alpha}{\partial q^i} \left. \frac{\partial q^i}{\partial t} \right|_{\mathbf{q}_0} \right) \sum_\beta f^\beta(t) \, b_\beta(\mathbf{q}) \, d\mu(\mathbf{q}) \tag{122}$$

$$= \sum_\beta L_\beta^\alpha \, f^\beta \tag{123}$$

$$L_\beta^\alpha := \int \frac{\partial b^\alpha}{\partial q^i} \left. \frac{\partial q^i}{\partial t} \right|_{\mathbf{q}_0} b_\beta(\mathbf{q}) \, d\mu(\mathbf{q}) \tag{124}$$

To obtain the time derivatives, we consider

$$\Omega = \dot{\mathbf{Q}} \, \mathbf{Q}^T \tag{125}$$

$$= \frac{\partial \mathbf{Q}}{\partial q^i} \left. \frac{\partial q^i}{\partial t} \right|_{\mathbf{q}_0} \mathbf{Q}^T \tag{126}$$

and perform a double contraction of Eq. 126 with the Levi-Civita tensor ε. Introducing appropriate abbreviations, this provides a linear system for the derivatives

$$\mathbf{v} \quad = \quad \left.\frac{\partial q^i}{\partial t}\right|_{\mathbf{q}_0} \mathbf{v}_i \tag{127}$$

$$\mathbf{v} \quad := \quad \varepsilon\left[\,\boldsymbol{\Omega}\,\right] \tag{128}$$

$$\mathbf{v}_i \quad := \quad \varepsilon\left[\,\frac{\partial \mathbf{Q}}{\partial q^i}\,\mathbf{Q}^{\mathrm{T}}\,\right] \tag{129}$$

For $[\mathbf{v}_1, \mathbf{v}_2, \mathbf{v}_3] \neq 0$ this system has the unique solution

$$\left.\frac{\partial q^i}{\partial t}\right|_{\mathbf{q}_0} = \frac{[\mathbf{v}, \mathbf{v}_j, \mathbf{v}_k]}{[\mathbf{v}_1, \mathbf{v}_2, \mathbf{v}_3]} \tag{130}$$

where (i, j, k) is a cyclic permutation of (1,2,3). As expected in view of Eq. 51, the matrix L only depends on $\mathbf{W}$ and $\mathbf{X}$.

The focus of this work is on the evolution of the crystallographic texture and its influence on the stress strain-rate relation. However, the procedure outlined in this section applies to an arbitrary choice of internal variables provided (1) the locally homogeneous process and micro-scale constitutive equation ensure the existence of a motion and (2) a complete set of base functions can be devised.

8 Summary

Summary. We have derived an alternative formulation of rigid perfectly viscoplastic polycrystals. The transition from single to polycrystal model is unique in that no additional parameters are required. The numerical results obtained hitherto agree well with the reference model but our approach reduces the computing time by several orders of magnitude. Since it requires the same input ($\mathbf{W}$ and $\mathbf{X}$) as the Sachs or Taylor model, it can be likewise implemented in FE codes. Moreover, the evolution equations in terms of arbitrary base functions and for a class of non-negative approximations have been derived.

Outlook. In forthcoming papers we shall (a) present details of the reduction of the computing time, (b) discuss the convergence of solutions (truncation error vs. truncation order) more rigorously, (c) include examples based on Taylor models for plane strain compression and simple shear deformation and (d) investigate the quadratic approximation in more detail.

References

Adams, B. L.; Boehler, J. P.; Guidi, M.; Onat, E. T.: Group theory and the representation of microstructure and mechanical behavior of polycrystals. *Journal of the Mechanics and Physics of Solids*, 40, 4, (1992), 723–737.

Bertram, A.: *Elasticity and plasticity of large deformations*. Springer, Berlin, 3rd edn. (2012).

Böhlke, T.: The Voigt bound of the stress potential of isotropic viscoplastic fcc polycrystals. *Archive of Mechanics*, 56, 6, (2004), 423–443.

Böhlke, T.: Application of the maximum entropy method in texture analysis. *Comp. Mat. Sci.*, 32, (2005), 276–283.

Böhlke, T.: Texture simulation based on tensorial Fourier coefficients. *Comp. Struct.*, 84, (2006), 1086–1094.

Böhlke, T.; Bertram, A.: Crystallographic texture induced anisotropy in copper: An approach based on a tensorial Fourier expansion of the codf. *Journal de Physique IV*, 105, (2003), 167–174.

Bunge, H.-J.: Zur Darstellung allgemeiner Texturen. *Z. Metallkde.*, 56, (1965), 872–874.

Elstrodt, J.: *Maß- und Integrationstheorie*. Springer, Berlin (2009).

Fritzen, F.; Böhlke, T.: Nonlinear homogenization using the nonuniform transformation field analysis. *Proc. Appl. Math. Mech.*, 11, (2011a), 519–522.

Fritzen, F.; Böhlke, T.: Nonuniform transformation field analysis of materials with morphological anisotropy. *Composite Science and Technology*, 71, (2011b), 433–442.

Gel'fand, I.; Minlos, R.; Shapiro, Z.: *Representations of the rotation and Lorentz groups and their applications.* Pergamon Press, Oxford (1963).

Guidi, M.; Adams, B. L.; Onat, E. T.: Tensorial representation of the orientation distribution function in cubic polycrystals. *Textures and Microstructures*, 19, (1992), 147–167.

Hielscher, R.; Mainprice, D.; Schaeben, H.: Material behavior: Texture and anisotropy. In: W. Freeden; M. Nashed; T. Sonar, eds., *Handbook of Geomathematics*, pages 973–1003, Springer-Verlag, Berlin (2010).

Hutchinson, J.: Bounds and self-consistent estimates for creep of polycrystalline materials. *Proc. R. Soc. Lond. A*, 348, (1976), 101–127.

Jaynes, E.: Information theory and statistical mechanics. *Phys. Rev.*, 106, (1957a), 620–630.

Jaynes, E.: Information theory and statistical mechanics ii. *Phys. Rev.*, 108, (1957b), 171–190.

Junk, M.; Budday, J.; Böhlke, T.: On the solvability of maximum entropy moment problems in texture analysis. *Mathematical Models and Methods in Applied Sciences*, 22(12).

Knezevic, M.; Al-Harbi, H.; Kalidindi, S.: Crystal plasticity simulations using discrete Fourier transforms. *Acta Materialia*, 57, (2009), 1777–1784.

Liu, B.; Raabe, D.; Roters, F.; Eisenlohr, P.; Lebensohn, R.: Comparison of finite element and fast Fourier transform crystal plasticity solvers for texture prediction. *Modelling Simul. Mater. Sci. Eng.*, 18.

Moler, C.; van Loan, C.: Nineteen dubious ways to compute the exponential of a matrix, twenty-five years later. *SIAM Review*, 45, 1, (2003), 3–49.

Sachs, G.: Zur Ableitung einer Fließbedingung. *Z. Verein dt. Ing.*, 72, (1928), 734–736.

Sam, D.; Onat, E. T.; Etingof, P.; Adams, B. L.: Coordinate free tensorial representation of the orientation distribution function with harmonic polynomials. *Text. Microstruct.*, 21, (1993), 233–250.

Taylor, G.: Plastic strain in metals. *J. Inst. Metals*, 62, (1938), 307–324.

Tsotsova, R.; Böhlke, T.: Effective flow potentials for anisotropic polycrystals. *Appl. Math. Mech.*, 9, Suppl.1, (2009a), 315–316.

Tsotsova, R.; Böhlke, T.: Representation of effective flow potentials for polycrystals based on texture data. *International Journal of Material Forming*, 2, Suppl.1, (2009b), 451–454.

van Houtte, P.: The use of a quadratic form for the determination of non-negative texture functions. *Textures and Microstructures*, 6, (1983), 1–20.

Address: Institut fuer Mechanik, Otto-von-Guericke-Universitaet, D-39106 Magdeburg, Germany
email: `jan.kalisch@ovgu.de`